Article

Syncytial Isopotentiality: An Electrical Feature of Spinal Cord Astrocyte Networks

Mi Huang [1,2]**, Yixing Du** [2]**, Conrad M. Kiyoshi** [2]**, Xiao Wu** [2,3]**, Candice C. Askwith** [2]**, Dana M. McTigue** [2] **and Min Zhou** [2,*]

[1] Department of Spine Surgery, Wuhan First Hospital, Wuhan 430022, China; huang.3155@osu.edu
[2] Department of Neuroscience, Ohio State University Wexner Medical Center, Columbus, OH 43210, USA; du.337@osu.edu (Y.D.); kiyoshi.1@osu.edu (C.M.K.); xiao.wu@osumc.edu (X.W.); askwith.1@osu.edu (C.C.A.); mctigue.2@osu.edu (D.M.M.)
[3] Department of Neurology, Wuhan First Hospital, Wuhan 430022, China
* Correspondence: zhou.787@osu.edu; Tel.: +1-614-366-9406

check for updates

Abstract: Due to strong electrical coupling, syncytial isopotentiality emerges as a physiological mechanism that coordinates astrocytes into a highly efficient system in brain homeostasis. Although this electrophysiological phenomenon has now been observed in astrocyte networks established by different astrocyte subtypes, the spinal cord remains a brain region that is still unexplored. In ALDH1L1-eGFP transgenic mice, astrocytes can be visualized by confocal microscopy and the spinal cord astrocytes in grey matter are organized in a distinctive pattern. Namely, each astrocyte resides with more directly coupled neighbors at shorter interastrocytic distances compared to protoplasmic astrocytes in the hippocampal CA1 region. In whole-cell patch clamp recording, the spinal cord grey matter astrocytes exhibit passive K^+ conductance and a highly hyperpolarized membrane potential of -80 mV. To answer whether syncytial isopotentiality is a shared feature of astrocyte networks in the spinal cord, the K^+ content in a physiological recording solution was substituted by equimolar Na^+ for whole-cell recording in spinal cord slices. In uncoupled single astrocytes, this substitution of endogenous K^+ with Na^+ is known to depolarize astrocytes to around 0 mV as predicted by Goldman–Hodgkin–Katz (GHK) equation. In contrast, the existence of syncytial isopotentiality is indicated by a disobedience of the GHK predication as the recorded astrocyte's membrane potential remains at a quasi-physiological level that is comparable to its neighbors due to strong electrical coupling. We showed that the strength of syncytial isopotentiality in spinal cord grey matter is significantly stronger than that of astrocyte network in the hippocampal CA1 region. Thus, this study corroborates the notion that syncytial isopotentiality most likely represents a system-wide electrical feature of astrocytic networks throughout the brain.

Keywords: astrocytes; spinal cord; gap junctions; electrical coupling; syncytial isopotentiality

1. Introduction

A distinctive feature of astrocytes lies in the establishment of the largest syncytial networks through gap junction coupling. The syncytial networks run through the entire central nervous system (CNS), including astrocytes in the spinal cord [1,2]. Over several decades, this unique anatomic attribute has sparked the speculation and exploration of the physiological mechanisms that enable astrocytes to indeed function as a system in the brain function [3,4]. One mechanism that was revealed in our recent study shows that strong electrical coupling enables hippocampal astrocytes to constantly equalize their membrane potentials so that a syncytial isopotentiality can be achieved [5]. Functionally, the dependence of syncytial isopotentiality for the operation of the K^+ spatial buffering was speculated over 20 years [6]. Now, our study

indeed showed that a sustained and highly efficient K^+ uptake driving force crucially depends on gap junctional coupling, which establishes syncytial isopotentiality [5].

Syncytial isopotentiality was initially identified from hippocampal astrocytes. Thereafter, the syncytial isopotentiality has been further uncovered as a broadly existing electrophysiological phenomenon in other parts of the brain, including protoplasmic astrocytes in the motor, sensory and visual cortical regions; cerebellar Bergman glia; velate astrocytes; and fibrous astrocytes in the *corpus callosum* [7]. The spinal cord constitutes a major portion of CNS, which connects the brain to the peripheral nervous system. However, it remains unknown whether syncytial isopotentiality also operates in astrocyte networks in this critical part of the brain. This question is important because astrocytes in different brain subregions vary in their cell morphology, spatial organization, association with different neuronal circuitries and gene expression [8–13]. Additionally, an early study, which used an elegant fluorescence after photo-bleaching (FRAP) method, showed that the cultured spinal cord astrocytes exhibited poor syncytial coupling compared to other brain regions [2].

To answer this question, we have examined the morphology, spatial organization pattern and syncytial isopotentiality expression in spinal cord grey matter. In doing so, confocal microscopy was used to examine the morphology of astrocytes and their spatial organizations in ALDH1L1-eGFP mice at a high resolution. The existence of syncytial isopotentiality was examined by our newly developed methodology, which involves the use of K^+-free/Na^+-containing recording pipette solutions [5].

We showed that astrocytes in cervical spinal cord grey matter are organized with more directly coupled neighbors at shorter interastrocytic distances compared to hippocampal astrocytes. This is associated with a higher strength of syncytial isopotentiality. This finding reinforces the notion that syncytial isopotentiality represents a general feature of astrocytic networks throughout the brain.

2. Materials and Methods

2.1. Animals

All experimental procedures were performed in accordance with a protocol that was approved by the Institutional Animal Care and Use Committee of The Ohio State University (2011A00000065-R2). All experiments were performed with the use of wild-type C57BL/J6 and BAC ALDH1L1-eGFP transgenic mice of both sexes at postnatal day (P) 15—21 [7,14,15]. Mice were housed in a 12-h light/dark cycle and temperature controlled (22 $\pm$ 2 °C) environment with *ad libitum* access to food and water.

2.2. Preparation of Acute Spinal Cord Slices

Mice were anesthetized with 8% chloral hydrate in 0.9% NaCl saline [16]. Spinal cord slices were prepared as previously described with modifications [17]. After deep anesthesia, the spinal cord was removed and placed into ice-cold oxygenated (95%O_2/5%CO_2) cutting artificial cerebrospinal fluid (aCSF) with reduced Ca^{2+} and increased Mg^{2+} (in mM: 125 NaCl, 3.5 KCl, 25 NaHCO$_3$, 1.25 NaH$_2$PO$_4$, 0.1 CaCl$_2$, 3 MgCl$_2$ and 10 glucose). The spinal cord was then transferred into a solid embedding-mold prepared by adding 4% low melt agar to the cutting aCSF, which was followed by the filling of the mold with liquid 2% agar dissolved in the cutting aCSF at ~35 °C. This mixture quickly solidified on ice. Several 400-μm sections were cut from the cervical regions using a Vibratome (MicroSlicer Zero 1N, Ted Pella, Redding, CA, USA) in ice-cold artificial cerebrospinal fluid (in mM: 125 NaCl, 25 NaHCO$_3$, 1.25 NaH$_2$PO$_4$, 3.5 KCl, 2 CaCl$_2$, 1 MgCl$_2$ and 10 glucose, osmolality, 295 $\pm$ 5 mOsm; pH of 7.3–7.4). The slices were allowed to recover from any damage caused by the preparation for at least 15 min at room temperature (RT) before electrophysiological recording.

2.3. Sulforhodamine 101 Staining

After recovery, spinal cord slices were transferred to a slice-holding basket containing 0.6 μM sulforhodamine 101 (SR101) in aCSF at 34 °C for 30 min. After this, the slices were transferred back to normal aCSF at RT before the experiment [14].

2.4. Confocal Imaging of Spinal Cord Astrocyte Syncytia

Anesthetized mice were cardially perfused with 4% paraformaldehyde (PFA) in 0.1 M phosphate-buffered saline (PBS). The 1-mm spinal cord cervical slices were sectioned and post-fixed in 4% PFA/0.1 M PBS at 4 °C overnight. Slices were incubated in a blocking solution, which consisted of 5% normal donkey serum and 0.1% Triton X-100 in PBS, for 24 h at RT. Images were acquired by confocal microscopy (SP8, Leica, Wetzlar, Germany).

2.5. Imaging Acquisition for Astrocyte Identification In Situ

An infrared differential interference contrast (IR-DIC) video camera was used to visualize the macroscopic structure of the spinal cord and astrocyte cell bodies for electrode placement and whole-cell patch clamp recording.

2.6. Electrophysiology

Individual spinal cord slices were transferred to the recording chamber and mounted on an Olympus BX51WI microscope (Center Valley, PA, USA) with constant oxygenated aCSF (2.0 mL/min) bath perfusion. Whole-cell patch clamp recordings were performed using a MultiClamp 700A amplifier and pClamp 9.2 software (Molecular Devices, Sunnyvale, CA, USA). Borosilicate glass pipettes (Warner Instrument, Hamden, CT, USA) were pulled from a Micropipette Puller (Model P-87, Sutter Instrument, Novato, CA, USA). The recording electrodes had a resistance of 3–5 MΩ when filled with the electrode solution that contained (in mM) 140 KCl (or NaCl), 1.0 MgCl$_2$, 0.5 CaCl$_2$, 10 HEPES, 5 EGTA, 3 Mg-ATP and 0.3 Na-GTP (pH = 7.25–7.30, 280 ± 5 mOsm). The physiological 140 KCl-containing pipette solution is referred to as [K$^+$]$_P$, whereas the K$^+$-free/140 mM NaCl-containing pipette solution is referred as [Na$^+$]$_P$ in this study. For whole-cell recording, the liquid junction potential was compensated prior to all recordings. The membrane potential (V_M) was read in I = 0 mode or continuously recorded under the current clamp mode in PClamp 9.2 program. To ensure the quality of current clamp recording, the input resistance (R_{in}) was periodically measured by "Resistance test" (a 63 pA/600 ms pulse) before and during the recording. Recordings with an initial R_{in} greater than 50 MΩ or R_{in} varied greater than 10% during recording were discarded. All the experiments were conducted at RT.

2.7. Chemical Reagents

All chemicals were purchased from Sigma-Aldrich (St. Louis, MO, USA).

2.8. Data Analyses

The patch clamp recording data were analyzed by Clampfit 9.0 (Molecular Devices). Statistical analysis was performed using Origin 8.0 (OriginLab, Northampton, MA, USA) or IBM SPSS Statistics 25.0 (IBM, Armonk, NY, USA). Results are given as means ± standard error of the mean (SEM).

3. Results

3.1. Spatial Organization of Astrocyte Syncytium in Cervical Spinal Cord

To visualize astrocytes and their spatial organization in spinal cord grey matter, the cervical sections of the spinal cord were prepared from ALDH1L1-eGFP mice (Figure 1). The interastrocytic distance and the number of the nearest neighbors for each individual astrocyte were quantitatively analyzed according to the procedure described in our previous reports [7,18].

For interastrocytic distance analysis, the distance between two astrocytes was measured between the nearest neighbors at the central points of the soma (Figure 1C). The grey matter astrocytes were spaced apart at an average of 30.1 ± 1.4 μm (*n* = 30 measurements from 3 slices). This distance is significantly shorter than the distance between astrocytes in the hippocampal CA1 region, which was found to be 39.5 μm in our recent report [7]. We further explored this by analyzing newly prepared hippocampal

CA1 syncytium. Consistently, astrocytes in hippocampal CA1 exhibited significantly longer interastrocytic distances than spinal cord grey matter as they were found to have an average interastrocytic distance of 41 ± 1.2 ($n = 30$ measurements from 3 slices, $p < 0.001$, image data not shown).

In the nearest neighbor analysis, a randomly chosen astrocyte is set as the reference cell and astrocytes were considered as the nearest neighbors if there was no intermediate astrocyte or a blood vessel between them (Figure 1D) [18]. Each astrocyte in spinal cord grey matter was directly coupled to 9.9 ± 0.3 astrocytes ($n = 9$ measurements from 3 slices), which was also significantly higher than the number of nearest neighbors of hippocampal CA1 astrocytes (8.7 ± 0.3; $n = 9$ measurements from 3 slices, $p < 0.01$).
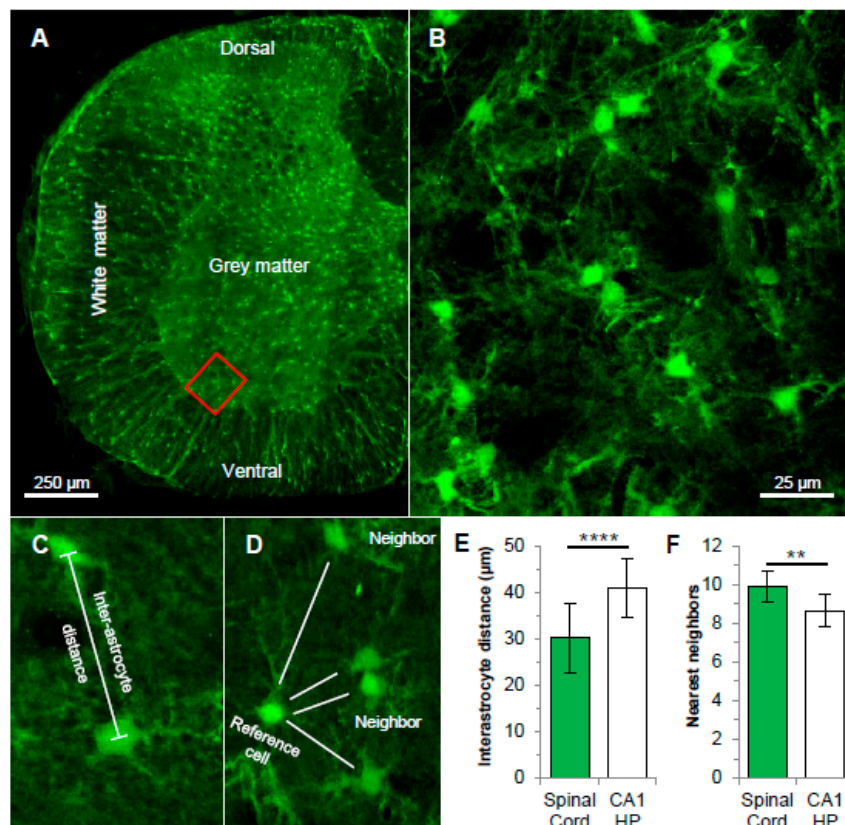

Figure 1. Astrocyte syncytial networks in the cervical spinal cord. (**A**) Confocal image of astrocyte networks in a cervical section of the spinal cord from ALDH1L1-eGFP mouse. (**B**) Astrocytes in a subfield of grey matter marked inside the red rectangle in (**A**) are shown in higher magnification. (**C,D**) Representations of astrocyte syncytium anatomical parameters, which are namely interastrocytic distance and the nearest neighbors as indicated. (**E,F**) In a comparison of the hippocampal CA1 (CA1 HP) region, spinal cord astrocytes show significantly shorter interastrocytic distances (**E**). Furthermore, each spinal cord astrocyte is coupled to ~9 nearest neighbors, which is ~1 more than hippocampal astrocyte. ** $p < 0.01$, **** $p < 0.001$.

Overall, astrocytes in the spinal cord grey matter are organized in a pattern that is distinct from the patterns of astrocytes in hippocampal CA1 and cortical regions. Specifically, each astrocyte is directly coupled to more surrounding neighbors at a shorter interastrocytic distance, which resembles the astrocyte networks that are established by velate astrocytes in the cerebellum [7].

3.2. Electrophysiological Properties of Grey Matter Astrocytes in the Spinal Cord

In acute spinal cord slices, astrocytes in the grey matter could be readily visualized under DIC (Figure 2A,B). Astrocytes can be identified based on the expression of eGFP in ALDH1L1-eGFP transgenic mice or positive staining to astrocytic marker SR101. A representative astrocyte identification based on SR101 staining is shown in Figure 2B,C. Astrocytes in the white matter could hardly be visualized and thus, we have focused on grey matter astrocytes for the following electrophysiological studies.

In whole-cell voltage clamp recording with a K^+-based solution, astrocytes exhibited a characteristic linear current–voltage (I–V) relationship membrane K^+ conductance or passive conductance (Figure 2C,D). This current profile was consistent with the findings of other studies that focused on spinal grey matter [19,20]. Furthermore, these astrocytes exhibit a relatively negative resting membrane potential of -80.8 ± 3.7 mV ($n = 9$) and a low input membrane resistance (R_{in}) of 21.1 ± 7.0 MΩ ($n = 5$). These electrophysiological features also resemble astrocytes in other brain regions, which are namely mature astrocytes in the hippocampus, cortical regions and cerebellum [7,21].
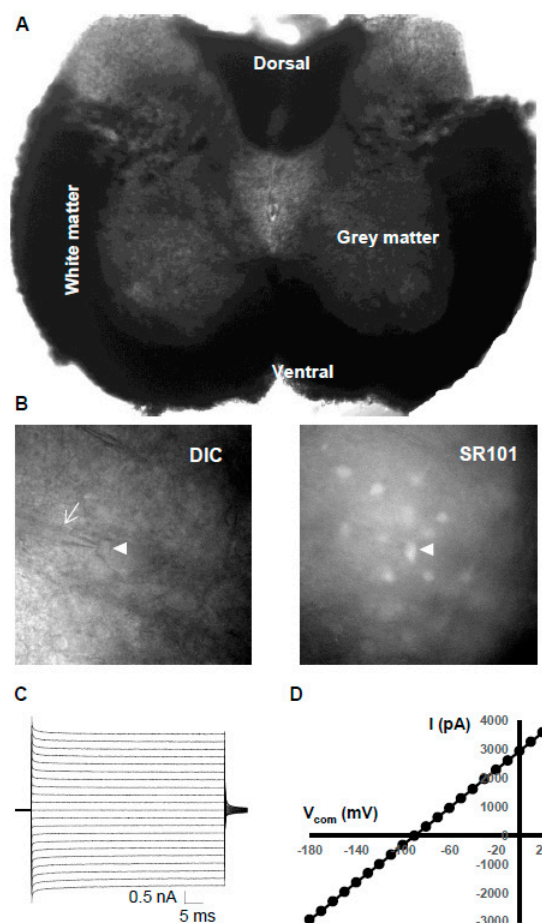

Figure 2. Electrophysiological properties of astrocytes in spinal cord grey matter. (**A**) Differential interference contrast (DIC) image of a cervical spinal cord slice. (**B**) An astrocyte in grey matter identified based on morphology during recording. Arrow and arrowhead point to the recording electrode and a recorded cell, respectively. The astrocytic identity of the recorded cell is confirmed by its sulforhodamine 101 (SR101) positive staining. (**C,D**) Whole-cell recording from an SR101 positively stained astrocyte. For whole-cell membrane current induction, the command voltages, which range from -180 mV to $+20$ mV at increments of 10 mV and duration of 50 ms, were delivered. This induced an ohmic behavioral passive K^+ membrane conductance characterized by a linear current-voltage (I–V) relationship.

3.3. Syncytial Isopotentiality—An Electrical Feature of Spinal Cord Astrocyte Networks

As a result of strong electrical coupling, astrocytes in various brain regions constantly equalize their membrane potential (V_M) so that a syncytial isopotentiality can be achieved [5,7]. Technically, the existence of syncytial isopotentiality can be readily detected by whole-cell membrane potential (V_M) recording with K^+-free/Na^+-containing electrode solutions ($[Na^+]_P$) [5]. Under this condition, dialysis of the recorded cell with $[Na^+]_P$ creates a "K^+-deficient astrocyte" inside a syncytial network (Figure 3A) and a V_M depolarization to ~0 mV is anticipated in the recorded cell. However, in various brain regions, this V_M depolarization can be largely suppressed by the physiological V_M of astrocytes in the associated syncytium. Consequently, a steady-state quasi-physiological V_M ($V_{M,SS}$) or syncytial isopotentiality remains throughout the recording [5,7]. As shown in Figure 3B, after the rupture of the membrane that switches on the whole-cell mode, the recorded V_M remained at a steady-state level throughout the recording with a $V_{M,SS}$ of -75.2 ± 1.1 ($n = 8$).
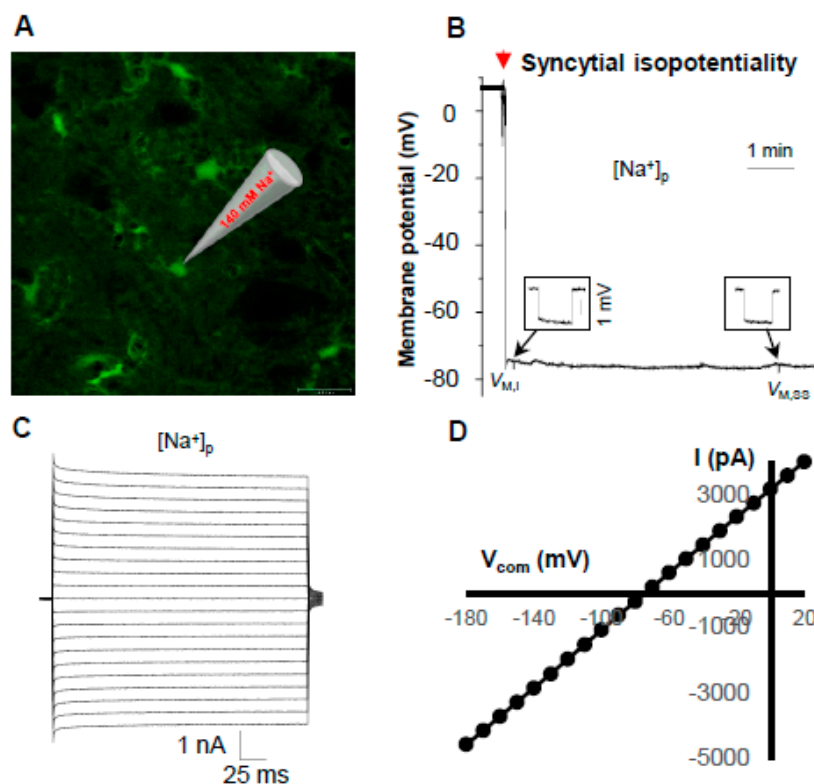

Figure 3. Syncytial isopotentiality in spinal cord grey matter. (**A**) A small field of astrocyte network in grey matter spinal cord revealed from an Aldh1L1-eGFP mouse for illustration of examination of syncytial isopotentiality with K^+-free/Na^+-containing electrode solution ($[Na^+]_p$). (**B**). Membrane potential (V_M) recorded from $[Na^+]_p$. After reaching a gigaohm formation, the break-in of the membrane, which is indicated by the red arrow, led to a rapid downward deflection of V_M toward the resting V_M. Thereafter, the V_M remained at a steady-state quasi-physiological level ($V_{M,SS}$) at around -75 mV, which indicated a strong electrical coupling of astrocytes that prevents the anticipated depolarization as predicted by Goldman–Hodgkin–Katz (GHK) equation. (**C**) In $[Na^+]_P$ recording, an absence of outward K^+ conductance is predicted by the GHK equation. However, the "missing" outward K^+ conductance was fully compensated for by the associated syncytium that resulted in a linear I–V K^+ conductance (**D**).

In an uncoupled "K^+-deficient astrocyte", the absence of outward conducting K^+ ions is anticipated to eliminate the outward K^+ conductance. In a syncytial coupled "K^+-deficient astrocyte", this "missing" outward K^+ conductance can be fully compensated for by its associated syncytium [5]. As shown in Figure 3C,D, in an experimentally created spinal cord "K^+-deficient astrocyte",

the syncytial coupling was indeed able to compensate for the missing outward K$^+$ conductance to a level so that the resultant linear I–V relationship did not differ from the recordings made with K$^+$ recording electrode solution (Figure 2D).

In summary, syncytial isopotentiality appears as a shared feature of astrocyte networks in spinal cord grey matter astrocytes. Functionally, a strong gap junction coupling provides spinal cord syncytium with the ability to effectively redistribute K$^+$ ions throughout the network.

4. Discussion

Now, syncytial isopotentiality has been identified in various brain regions, including the hippocampus, visual, sensory and motor cortex, cerebellar and *corpus callosum* [5,7]. Nevertheless, the spinal cord remains a significant portion of the CNS that has still not been explored. In the present study, this issue was examined using acute slices prepared from the cervical sections of the spinal cord. We showed that syncytial isopotentiality is a shared feature of astrocyte networks in spinal cord grey matter.

4.1. Anatomical Characteristics of Grey Matter Spinal Cord Astrocyte Networks

Astrocytes are known to establish the largest syncytial networks through gap junction coupling in the brain. This distinct anatomic attribute has led to the speculation that astrocytes may act as a system in basic and advanced brain functions [3]. In the search for the mechanisms that enable astrocytes to function at network system levels, syncytial isopotentiality has been revealed as a network physiological mechanism that coordinates astrocytes into a highly efficient system for homeostatic regulation of K$^+$ concentration in the brain [5].

Now, the study of astrocyte heterogeneity has expanded from early cytoarchitecture to embryonic origins, gene expression and physiological functions [22,23]. In our recent study, we showed that the morphology and spatial organization partners vary from brain region to brain region. However, syncytial isopotentiality is still a general feature of astrocyte syncytial networks [7]. Despite that, a question that is not fully understood is the existence of syncytial isopotentiality in the entire brain and how this is associated with the anatomy of the astrocyte network. An early study from cultured spinal cord astrocytes showed that spinal cord astrocytes exhibited a rather poor gap junction coupling [2]. However, whether this early observation holds true to native spinal cord astrocytes remains unknown.

In our morphological analysis of syncytial organization in the grey matter of the spinal cord, we found that the morphology of individual astrocytes does not differ between the spinal cord and protoplasmic astrocytes in other parts of the brain, such as the hippocampus and visual cortex (data not shown). However, astrocytes in the spinal cord grey matter are characterized by having more surrounding neighbors and a significantly shorter interastrocytic distance compared to those in the hippocampal CA1 region and visual cortex. Interestingly, these features resemble the syncytial network established by velate astrocytes in the cerebellar molecular layer [7].

4.2. Spinal Cord Astrocytes Establish Syncytial Isopotentiality in Their Networks

Extending from our previous studies, the present findings from spinal cord grey matter astrocytes further corroborate the notion that syncytial isopotentiality is a general feature of astrocyte networks. Interestingly, the strength of syncytial isopotentiality in spinal cord astrocytes appears to be stronger than that of hippocampal astrocytes, which was indicated by a more negative $V_{M,SS}$. This is correlated with a shorter interastrocytic distance and one more nearest neighbor. However, although the spinal cord astrocytes share a similar interastrocytic distance and nearest neighbors with velate astrocytes, the latter exhibits a weaker strength of syncytial isopotentiality than the spinal cord. Interestingly, spinal cord astrocytes share a comparable interastrocytic distance and strength of syncytial isopotentiality to astrocytes in layer I motor, sensory and visual cortex, but appear to have one more nearest neighbor.

Previously, we have demonstrated that a minimum of 7–9 directly coupled neighbors is sufficient for establishing syncytial isopotentiality [5]. However, it remains unknown how the fine-tuning of coupling strength is achieved and regulated. From a structural standing point, these observations again stress the importance of the identification of the generic astrocyte-connectome, which underpins syncytial isopotentiality. This could be better answered by electron microscopy (EM) reconstruction of the adjacent astrocytes in conjunction with computational modeling in future studies.

4.3. Pathological Implications Affecting Astrocyte Syncytial Isopotentiality

Astrocytes become reactive in response to neurological injuries and diseases by exhibiting changes in cell morphology, genetic and molecular expression [24]. The expression of gap junction channels and functional dye coupling are reported to be affected in various disease models [25]. A question that yet unknown is how the disease conditions alter syncytial isopotentiality in the spinal cord.

It has been shown that connexin 43 (Cx43), but not connexin 30 (Cx30), plays a critical role in the development of chronic neuropathic pain following spinal cord injury [26]. In compression injuries, Cx43 undergo a marked alteration in localization and expression [27]. These observations suggest that pathological conditions may alter the spatial organization of astrocyte syncytium in the spinal cord, which may subsequently disrupt the physiological syncytial isopotentiality. Nevertheless, no study has yet been carried out to determine a causal relationship between syncytial isopotentiality and the pathogenesis of various types of neurological disorders in the spinal cord.

Conflicts of Interest: The authors declare no conflict of interest.

References

1. Scemes, E.; Suadicani, S.O.; Spray, D.C. Intercellular communication in spinal cord astrocytes: Fine tuning between gap junctions and P2 nucleotide receptors in calcium wave propagation. *J. Neurosci.* **2000**, *20*, 1435–1445. [CrossRef] [PubMed]
2. Lee, S.H.; Kim, W.T.; Cornell-Bell, A.H.; Sontheimer, H. Astrocytes exhibit regional specificity in gap-junction coupling. *Glia* **1994**, *11*, 315–325. [CrossRef] [PubMed]
3. Nimmerjahn, A.; Bergles, D.E. Large-scale recording of astrocyte activity. *Curr. Opin. Neurobiol.* **2015**, *32*, 95–106. [CrossRef] [PubMed]
4. Verkhratsky, A.; Nedergaard, M. Physiology of Astroglia. *Physiol. Rev.* **2018**, *98*, 239–389. [CrossRef] [PubMed]
5. Ma, B.; Buckalew, R.; Du, Y.; Kiyoshi, C.M.; Alford, C.C.; Wang, W.; McTigue, D.M.; Enyeart, J.J.; Terman, D.; Zhou, M. Gap junction coupling confers isopotentiality on astrocyte syncytium. *Glia* **2016**, *64*, 214–226. [CrossRef] [PubMed]
6. Muller, C.M. Gap-junctional communication in mammalian cortical astrocytes: Development, modifiability and possible functions. In *Gap Junctions in the Nervous System*; Spray, D.C., Ed.; RG Landes Company: Austin, TX, USA, 1996; pp. 203–212.
7. Kiyoshi, C.M.; Du, Y.; Zhong, S.; Wang, W.; Taylor, A.T.; Xiong, B.; Ma, B.; Terman, D.; Zhou, M. Syncytial isopotentiality: A system-wide electrical feature of astrocytic networks in the brain. *Glia* **2018**, in press.
8. Houades, V.; Rouach, N.; Ezan, P.; Kirchhoff, F.; Koulakoff, A.; Giaume, C. Shapes of astrocyte networks in the juvenile brain. *Neuron Glia Biol.* **2006**, *2*, 3–14. [CrossRef] [PubMed]
9. Houades, V.; Koulakoff, A.; Ezan, P.; Seif, I.; Giaume, C. Gap junction-mediated astrocytic networks in the mouse barrel cortex. *J. Neurosci.* **2008**, *28*, 5207–5217. [CrossRef] [PubMed]
10. Roux, L.; Benchenane, K.; Rothstein, J.D.; Bonvento, G.; Giaume, C. Plasticity of astroglial networks in olfactory glomeruli. *Proc. Natl. Acad. Sci. USA* **2011**, *108*, 18442–18446. [CrossRef] [PubMed]

11. Nadarajah, B.; Thomaidou, D.; Evans, W.H.; Parnavelas, J.G. Gap junctions in the adult cerebral cortex: Regional differences in their distribution and cellular expression of connexins. *J. Comp. Neurol.* **1996**, *376*, 326–342. [CrossRef]

12. Morel, L.; Chiang, M.S.R.; Higashimori, H.; Shoneye, T.; Iyer, L.K.; Yelick, J.; Tai, A.; Yang, Y. Molecular and Functional Properties of Regional Astrocytes in the Adult Brain. *J. Neurosci.* **2017**, *37*, 8706–8717. [CrossRef] [PubMed]

13. Zhang, Y.; Barres, B.A. Astrocyte heterogeneity: An underappreciated topic in neurobiology. *Curr. Opin. Neurobiol.* **2010**, *20*, 588–594. [CrossRef] [PubMed]

14. Zhong, S.; Du, Y.; Kiyoshi, C.M.; Ma, B.; Alford, C.C.; Wang, Q.; Yang, Y.; Liu, X.; Zhou, M. Electrophysiological behavior of neonatal astrocytes in hippocampal stratum radiatum. *Mol. Brain* **2016**, *9*, 34. [CrossRef] [PubMed]

15. Yang, Y.; Vidensky, S.; Jin, L.; Jie, C.; Lorenzini, I.; Frankl, M.; Rothstein, J.D. Molecular comparison of GLT1+ and ALDH1L1+ astrocytes in vivo in astroglial reporter mice. *Glia* **2011**, *59*, 200–207. [CrossRef] [PubMed]

16. Wang, W.; Putra, A.; Schools, G.P.; Ma, B.; Chen, H.; Kaczmarek, L.K.; Barhanin, J.; Lesage, F.; Zhou, M. The contribution of TWIK-1 channels to astrocyte K(+) current is limited by retention in intracellular compartments. *Front. Cell. Neurosci.* **2013**, *7*, 246. [CrossRef] [PubMed]

17. Olsen, M.L.; Higashimori, H.; Campbell, S.L.; Hablitz, J.J.; Sontheimer, H. Functional expression of Kir4.1 channels in spinal cord astrocytes. *Glia* **2006**, *53*, 516–528. [CrossRef] [PubMed]

18. Xu, G.; Wang, W.; Kimelberg, H.K.; Zhou, M. Electrical coupling of astrocytes in rat hippocampal slices under physiological and simulated ischemic conditions. *Glia* **2010**, *58*, 481–493. [CrossRef] [PubMed]

19. Ficker, C.; Rozmer, K.; Kato, E.; Ando, R.D.; Schumann, L.; Krugel, U.; Franke, H.; Sperlagh, B.; Riedel, T.; Illes, P. Astrocyte-neuron interaction in the substantia gelatinosa of the spinal cord dorsal horn via P2X7 receptor-mediated release of glutamate and reactive oxygen species. *Glia* **2014**, *62*, 1671–1686. [CrossRef] [PubMed]

20. Minkel, H.R.; Anwer, T.Z.; Arps, K.M.; Brenner, M.; Olsen, M.L. Elevated GFAP induces astrocyte dysfunction in caudal brain regions: A potential mechanism for hindbrain involved symptoms in type II Alexander disease. *Glia* **2015**, *63*, 2285–2297. [CrossRef] [PubMed]

21. Du, Y.; Ma, B.; Kiyoshi, C.M.; Alford, C.C.; Wang, W.; Zhou, M. Freshly dissociated mature hippocampal astrocytes exhibit similar passive membrane conductance and low membrane resistance as syncytial coupled astrocytes. *J. Neurophysiol.* **2015**, *113*, 3744–3750. [CrossRef] [PubMed]

22. Ben Haim, L.; Rowitch, D.H. Functional diversity of astrocytes in neural circuit regulation. *Nat. Rev. Neurosci.* **2017**, *18*, 31–41. [CrossRef] [PubMed]

23. Bayraktar, O.A.; Fuentealba, L.C.; Alvarez-Buylla, A.; Rowitch, D.H. Astrocyte development and heterogeneity. *Cold Spring Harb. Perspect. Biol.* **2014**, *7*, a020362. [CrossRef] [PubMed]

24. Liddelow, S.A.; Barres, B.A. Reactive Astrocytes: Production, Function, and Therapeutic Potential. *Immunity* **2017**, *46*, 957–967. [CrossRef] [PubMed]

25. Giaume, C.; Koulakoff, A.; Roux, L.; Holcman, D.; Rouach, N. Astroglial networks: A step further in neuroglial and gliovascular interactions. *Nat. Rev. Neurosci.* **2010**, *11*, 87–99. [CrossRef] [PubMed]

26. Chen, M.J.; Kress, B.; Han, X.; Moll, K.; Peng, W.; Ji, R.R.; Nedergaard, M. Astrocytic CX43 hemichannels and gap junctions play a crucial role in development of chronic neuropathic pain following spinal cord injury. *Glia* **2012**, *60*, 1660–1670. [CrossRef] [PubMed]

27. Theriault, E.; Frankenstein, U.N.; Hertzberg, E.L.; Nagy, J.I. Connexin43 and astrocytic gap junctions in the rat spinal cord after acute compression injury. *J. Comp. Neurol.* **1997**, *382*, 199–214. [CrossRef]